Journal of Sound and Vibration 377 (2016) 1–21

Contents lists available at ScienceDirect

Journal of Sound and Vibration

journal homepage: www.elsevier.com/locate/jsvi

Optimal vibration control and co-design of very flexible actuated structures

S. Maraniello, R. Palacios *

Department of Aeronautics, Imperial College, London SW7 2AZ, United Kingdom

ARTICLE INFO

Article history:
Received 5 September 2015
Received in revised form
27 April 2016
Accepted 11 May 2016
Handling Editor: D.J. Wagg
Available online 24 May 2016

Keywords:
Vibration control
Optimization
Co-design
Control vector parametrisation
Single-shooting
Geometrically-nonlinear beams

ABSTRACT

The single shooting method is applied to the optimal control and combined structural and control design (co-design) of very flexible beams. The objective is to assess feasibility, advantages and limitations of an integrated design approach when dealing with actuated structures exhibiting large oscillations and, more generally, strongly nonlinear couplings. A gradient based approach is proposed for the large design space defined by both the optimal control and co-design problems. Numerical studies are presented for the case of a very flexible actuated pendulum with large rigid-body motion. The impact of local (B-splines) and global (discrete sines) set of basis functions is investigated for increasing levels of actuation authority, showing the importance of the time–frequency resolution of the parametrisation on the convergence properties and outcome quality of the process. Locking between control and structural disciplines around specific design points is found, thus highlighting the disadvantage of a sequential design approach. Simultaneous designing of control law and structure is seen, instead, to explore efficiently larger regions of the design space.

1. Introduction

While actively controlled structures generally provide better vibration characteristics than non-controlled, or passive, ones, the integration of the controller usually comes late in the design process. Their design typically relies on a sequential approach: the structure is initially sized for passive response and an active control is introduced only in a later stage, after the main features of the system have been established [1]. Looking at the structural design process from the perspective of a multidisciplinary optimisation (MDO) problem, there is substantial evidence that this approach is likely to generate only sub-optimal design points. For a true optimum, structural properties and control should be designed simultaneously, thus leading to the concept of combined design or co-design [1–3].

The advantages of a combined control and structural optimisation have long been proved in space structures design [4,5], robotics [6], and noise and vibration control [7,8]. These studies were based on a linear representation of the closed-loop system dynamics, which facilitated the approach to the design. Asada et al. [6], for instance, directly manipulated the position of the closed-loop system eigenvalues, while Rao [5] expressed the control gains in terms of the system energy

* Correspondence to: Room 355, Roderic Hill Building, South Kensington Campus, United Kingdom. Tel.: +44 20 7594 5075.
E-mail address: rpalacio@imperial.ac.uk (R. Palacios).

http://dx.doi.org/10.1016/j.jsv.2016.05.018
0022-460X/

properties. In this sense, the work from Onoda and Haftka [4] best fits the modern idea of combined design, as, aside from exploring a nested approach similar to that presented by Rao [5], they also optimised the system simultaneously with respect to optimiser gains and structural design parameters.

When dealing with the dynamics of structures outside the linear regime, however, integrating the design approaches becomes a much more challenging task. Common MDO architectures, in fact, rarely allow to take advantage of the fact that the control is inherently dependent on the evolution of a system in time [1]. The larger computational cost associated to a time-dependent nonlinear analysis is, therefore, not balanced by the optimisation approach, resulting in relatively inefficient architectures. Co-design studies dealing with complex structural dynamic models have been required, therefore, to reduce the analysis cost, either using metamodels [9] or limiting the size of the systems [10,11]. Nonlinear systems arising from the coupling of FEM with other disciplines, e.g. for aeroservoelasticity studies, have also required reduced-order models and linearised formulations [12,13].

Soft robotic manipulators [14], high-altitude long-endurance (HALE) aircraft wings or large horizontal axis wind turbine (HAWT) blades are all highly flexible structures in which possibly large deformations can lead to a nonlinear dynamical behaviour. As most of the critical operating conditions of these systems — both in terms of loading and stability — are associated with unsteady phenomena, an accurate representation of the coupling between structure and control system is a necessary, but not sufficient, condition to achieve optimal designs. Structural properties and control system should, in fact, be designed simultaneously while ensuring a balanced modelling fidelity between the disciplines.

Focusing on this aspect, this work aims to provide relevant guidelines for the co-design of slender, active structures. From a structural perspective, the analysis of these systems introduces nonlinearities when dealing with large geometrical deformations and couplings between rigid-body and flexible modes dynamics [15–17]. From a control system perspective, open-loop analysis will be considered. In real life applications, the control of actuated structures needs to be addressed in the presence of disturbances, thus requiring a feedback control and a closed-loop analysis. A deterministic open-loop analysis, in which the control has full authority on the system behaviour, remains, however, a necessary first step in the design process.

Optimal control problems can be solved through an optimise-discretise approach, in which an optimality condition is enforced on the equations describing the system dynamics [18]. However, in actual applications, the system is often too complex to apply optimality principles. A common way around this problem is to parametrise the control signal (direct methods). Single and multiple shooting methods, in particular, are directly linked to single and multidisciplinary optimisation [1,19]: once a parametrisation is chosen, the coefficients of the parametrisation are directly handled by the optimisation algorithm and there is no formal difference, at the optimiser level, between closed-loop system gain optimisation and open-loop optimal control solution.

While single and multiple shooting have been successfully used in many optimal control problems, an understanding on how these methods may apply to the control of active, strongly nonlinear, structures is a required step to assess the feasibility of their integration in a co-design framework. A first question to address is thus *how* to find the optimal actuation. When using medium-to-high fidelity models and dealing with dynamics, in particular, a global reconstruction of the design space via a zero-order optimisation method is, in general, not a feasible solution. Several authors, however, have showed that shooting methods can successfully be used in conjunction with gradient based optimisers to define control laws [20,21]. In this respect, the most common approach is to use piecewise constant or linear representations to parametrise the control signal [22].

The single shooting (or control vector parametrisation, CVP) method can be integrated in a pre-existing MDO architecture with relatively little effort. This approach, however, has to be further explored when dealing with co-design problems. In particular, as the optimisation relies on a gradient based method, it is important to assess how the smoothness of the design space is impacted when moving from optimal control to combined design. This also implies an assessment on how *large* changes in the design space can be.

In this work, a coupled flexible-rigid body dynamics model, based on a geometrically exact beam description, has been embedded in an optimisation framework. Applying the CVP technique, the actuation on the structure has been written as an optimal control problem using both a local (B-spline) and a global (discrete sine series, DSS) parametrisation (Section 2). The methodology is used to control the dynamics of a very flexible pendulum, modelled as a beam in hinged configuration and exhibiting large deformations (Section 3.1). As the pendulum flexibility increases, not only larger deformations arise, but the level of coupling between rigid and flexible modes also increases. Conceptually, therefore, this problem has many analogies to that of the control of a very flexible manipulator or to the trajectory tracking of a flexible aircraft in calm air. In particular, the impact of several factors — namely the level of nonlinearities, the problem formulation and the parametrisation used — on the optimal control results have been assessed in Sections 3.2 and 3.3.

The active system co-design problem is then addressed (Section 4). Due to the high level of coupling between control and structure, a multidisciplinary feasible (MDF) architecture is used [3] . The implication of different modelling choices for the actuation is shown and guidelines for the co-design process of structures exhibiting strong nonlinear dynamics are finally provided.

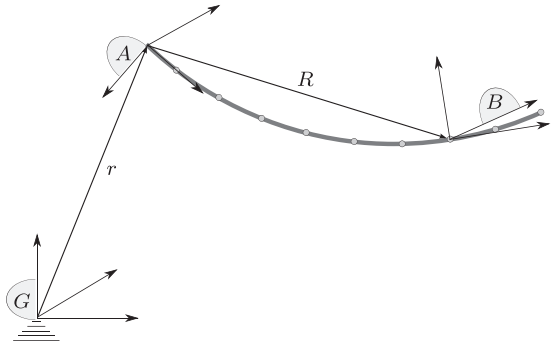

Fig. 1. Definition of frames of reference over the very flexible structure.

2. Methodology

The application of the single-shooting is tested for the control and co-design of very flexible, slender, partially supported structures. In particular, it is assumed that these may exhibit large deformations, i.e. comparable in magnitude with their largest dimension. This section starts, therefore, presenting a structural model with coupled rigid-flexible body dynamics (Section 2.1). The optimal control problem is then addressed, with Section 2.2 providing a brief introduction to direct methods for nonlinear optimal control: the single shooting method, and the way this can be extended to co-design, is here presented. The parametrisations implemented in this work are discussed in more detail in Section 2.3. An overview of the optimisation framework built for both the control and co-design is finally given in Section 2.4.

2.1. Rigid-flexible body dynamic model

For modelling slender, flexible structures, a geometrically exact beam model (GEBM) with coupled rigid-flexible body dynamics is used [23,24]. The model is here briefly described using the notation introduced in Ref. [25]; frame of references (FoRs) and relevant vectors are shown in Fig. 1. The rigid body dynamics is expressed in terms of translational (v_A) and rotational (ω_A) velocity vectors of a FoR attached to the body, A, with respect to the ground FoR G. Subscripts stand for the FoR in which quantities are projected.

Local deformations are assumed to be small, thus a linear material model is used. Force and moment strains are written in terms of the position, $R_A(s)$, and the Cartesian rotation vector, $\Psi(s)$, associated to a local FoR B, defined along a curvilinear coordinate s [23]. The coupled nonlinear flexible/rigid body dynamics is finally expressed using:

$$M(\eta)\begin{Bmatrix}\ddot{\eta}\\ \dot{\beta}\end{Bmatrix}+\begin{Bmatrix}Q^s_{\text{gyr}}(\eta,\dot{\eta},\beta)\\ Q^r_{\text{gyr}}(\eta,\dot{\eta},\beta)\end{Bmatrix}+\begin{Bmatrix}Q^s_{\text{stif}}(\eta)\\ 0\end{Bmatrix}=\begin{Bmatrix}Q^s_{\text{ext}}(\eta,\zeta,t)\\ Q^r_{\text{ext}}(\eta,\zeta,t)\end{Bmatrix}, \tag{1}$$

where $\beta^T=\{v_A^T,\omega_A^T\}$, η is a vector containing nodal rotation and displacements, $M(\eta)$ is the mass matrix, and Q_{gyr}, Q_{stif}, Q_{ext} are, respectively, gyroscopic, stiffness and external forcing terms. The latter includes control inputs and gravitational forces. For the coupled flexible-rigid body dynamics solution, the orientation of the body-attached FoR A with respect to the ground FoR G is required. This is expressed in terms of quaternions such that $\zeta^T=\{\zeta_0,\zeta_v^T\}$. The scalar ($\zeta_0$) and vector ($\zeta_v$) parts of ζ are obtained via integration of body-attached FoR angular velocity, ω_A, according to [26]:

$$\dot{\zeta}_0=-\frac{1}{2}\omega_A^T\zeta_v,\quad \dot{\zeta}_v=-\frac{1}{2}\left(\zeta_0\omega_A-\tilde{\omega}_A\zeta_v\right), \tag{2}$$

where ($\tilde{}$) is the skew symmetric matrix operator. Spherical joint boundary conditions (BCs) have been implemented by setting the translational velocity of the FoR A, v_A, to be zero. Hinge BCs can be derived similarly, allowing rotations only along one axis.

2.2. From optimal control to co-design

In general, an optimal control problem can be seen as an optimisation problem with a design variable, the control input u, that is a time-dependent function:

$$\begin{aligned}\text{min.}\quad & I=I(u,y,\dot{y})\\ \text{w.r.t.}\quad & u(t),y(t)\\ \text{s.t.}\quad & c(u,y)\geq 0\\ & R(t,u,y,\dot{y})=0\end{aligned} \tag{3}$$

In problem (3) y is the state of the system, I is the cost functional to minimise and c are the design constraints. The set of equations R *refers* to the coupled rigid-flexible body dynamics Eqs. (1) and (2) over the time horizon $[0,T]$. The design constraints, $c=\{c_o,c_c\}$, are divided into a set of control specific (c_c) and general (c_o) design requirement. The first set includes constraints associated to the control input u: in this work, bound constraints of the form

$$\begin{matrix} u(t)\geq u_L(t) \\ u(t)\leq u_H(t) \end{matrix}, \quad t\in[0,T], \tag{4}$$

as well as initial and terminal conditions, are enforced. The second set is instead associated to any other requirement on system performance.

While analytical tools for the solution of problem (3), such as Pontryagin's maximum principle, are available, they are too complex to be used for the control of large nonlinear systems [22]. The alternative are direct methods, in which the control function is discretised in time and expressed in terms of a coefficient vector x_c, i.e. $u(t)\rightarrow u(x_c)$. In direct transcription (DT) or direct simultaneous methods, also the state is discretised in time and treated as a design variable. The optimiser, therefore, handles problem (3) directly, simultaneously solving physics and actuation. In a MDO context, this approach would be referred to as an all-at-once or simultaneous analysis and design (SAND) [3]. DT methods can explore infeasible and unstable states, thus possibly leading to faster convergence, but they introduce a large number of design variables and, in MDO problems, may also have convergence issues. If Eq. (1) is solved at each iteration for the state, problem (3) can be recast in the form of a multidisciplinary feasible architecture:

$$\begin{aligned} \text{min.}\quad & I=I(x_c,y(x_c),\dot{y}(y,x_c)) \\ \text{w.r.t.}\quad & x_c \\ \text{s.t.}\quad & c_o(x_c,y(x_c))\geq 0 \\ & c_c(x_c,y(x_c))\geq 0 \end{aligned} \tag{5}$$

where the dependency of the state on the control, $y=y(x_c)$, has been explicitly stated. This approach is referred to as control vector parametrisation (CVP) or single-shooting method: while a solution to Eq. (1) has to be found at each optimisation, the size of the problem is reduced to its minimum.

The extension of problem (5) to a MDO problem that simultaneously optimises control action and structural properties is straightforward and only requires the inclusion of a set of structural design parameters, x_s, and constraints, c_s:

$$\begin{aligned} \text{min.}\quad & I=I(x_c,x_s,y(x_c,x_s),\dot{y}(y,x_c,x_s)) \\ \text{w.r.t.}\quad & x_c,x_s \\ \text{s.t.}\quad & c_o(x_c,x_s,y(x_c,x_s))\geq 0 \\ & c_c(x_c,x_s,y(x_c,x_s))\geq 0 \\ & c_s(x_c,x_s,y(x_c,x_s))\geq 0 \end{aligned} \tag{6}$$

This is the description that will be used in this work.

2.3. Control parametrisation

In the single shooting approach, the control signal is expressed as a linear combination of N_c basis functions, $\phi_n(t)$, defined over the time horizon $[0,T]$:

$$u=\sum_{n=1}^{N_c} x_{cn}\,\phi_n(t) \tag{7}$$

In most optimal control problems, a piecewise constant parametrisation is used: in addition to being easy to implement, that scheme offers good convergence properties [22]. However, to describe the movement of typical control actuators on a relatively large time domain, piecewise constant or linear parametrisations would lead to set of basis functions of substantial size. While from a computational point of view adjoint methods can deal effectively with an increased number of design variables, these present the additional development cost of building the adjoint model itself. Furthermore, the larger the basis size, the higher are the frequencies that the parametrisation can reproduce: a smoothing of the control signal to avoid unrealistically steep changes would, therefore, be required, either enforcing additional constraints on the control rate of change or smoothing the gradient itself.

With the purpose of modelling smooth actuation signals while limiting the number of coefficients used to parametrise the control, N_c, only C^1 continuous or higher parametrisations are considered for this work. As the dynamics of structures is strongly linked to the frequency of excitations of external disturbances and control forces (see also Sections 3 and 4), it is natural to use a parametrisation that can be easily linked to the frequency range of the control. An obvious candidate is the discrete Fourier series or, for control signals with $u(0)=u(T)=0$, discrete sine series (DSS) obtained as

$$\phi_n(t)=\sin 2\pi f_n t \quad \text{with: } f_n=n\,f_0,\ f_0=\frac{1}{2T} \tag{8}$$

The discrete Fourier series and the DSS have both the advantage of allowing a direct control of the maximum actuation frequency of the control. While sine and cosines are globally defined in time, however, they are collocated in the frequency domain, each harmonic being associated to a specific frequency f_n (see Eq. (8)). While this does not pose an issue in terms of

reconstruction properties,[1] a poor frequency resolution can be a penalty during the sensitivity analysis required to solve the optimal control problem (5) via a gradient based approach. When using a DSS parametrisation, in fact, the nth term of the cost function gradient, $\mathrm{d}I/\mathrm{d}x_{cn}$, with x_{cn} defined as in Eq. (7), represents the sensitivity of the cost function I with respect to a change in magnitude of the nth harmonic parametrising the control u: while affecting the whole time domain, this is localised at the frequency f_n.

The duality frequency vs. time resolution is a well known problem in signal and image processing [27]. In this sense, local basis functions can provide more flexibility in terms of capturing relevant frequency content of the structural dynamics response, particularly when large geometrical deformations imply changes in the system features (e.g. its natural frequencies) with time. To investigate this, B-splines have additionally been chosen for their smoothness properties. A set of B-splines basis functions of order p can be built recursively over a set of N_τ control points τ_n as [20]:

$$\phi_n^{(0)}(t) = \begin{cases} 1 & \text{if } \tau_n < t < \tau_{n+1} \\ 0 & \text{else} \end{cases} \tag{9}$$

and

$$\phi_n^{(p)}(t) = \frac{t-\tau_n}{\tau_{n+p}-\tau_n}\phi_n^{(p-1)}(t) + \frac{\tau_{n+p+1}-t}{\tau_{n+p+1}-\tau_{n+1}}\phi_{n+1}^{(p-1)}(t), \quad p>0 \tag{10}$$

Note that, if N_τ control points are used, the number of spline basis required is $N_c = N_\tau + p - 1$. Third-order B-splines were found to provide good and smooth reconstructions for the applications in this work.

The frequency range of actuation can be regulated by noticing that, in order to capture a maximum frequency $f_{\max}$, a spacing between control points $\Delta\tau = 1/(2f_{\max})$ is necessary (Nyquist criterion). It results that, fixed a $f_{\max}$ value, DSS and B-splines basis have comparable size and similar reconstruction properties, although it should be noted that the frequency spectrum of each spline basis has a smooth decay to zero towards $f_{\max}$. As it will be shown in Section 3.3, this means that harmonic components whose frequencies near $f_{\max}$ are not reconstructed accurately. While local in time, however, spline basis have a distributed frequency content, thus providing opposite properties to the DSS basis during a sensitivity analysis.

2.4. Optimisation framework

In line with Ref. [20,21] a standard quasi-Newton method, the SLSQP optimisation algorithm [28], has been used to solve both the nonlinear optimal control problem and the co-design optimisation. The GEBM with coupled flexible-rigid body dynamics from an in-house aeroelastic simulation environment [29,25] has been embedded in an optimisation framework built using OpenMDAO [30]. The implementation is monolithic and uses finite differences for the gradient evaluation.

Optimal control and co-design are solved using both DSS and B-splines. For both basis, the bound constraints in Eq. (4) are enforced by oversampling the control signal. In all the problems considered, cost and constraint functions, as well as design parameters, are scaled to achieve comparable orders of magnitude. If all the constraints are verified, the optimisation process is stopped whenever the relative change in cost and constraints is below a tolerance value of 0.1 percent.

3. Numerical studies on optimal control

The methodology presented in Section 2 is verified for the control of a very flexible actuated pendulum first proposed by Wang and Yu [31]. The pendulum is modelled as a very flexible beam and can undergo large rigid body rotations and geometrical deformations. Being fully deterministic — as no external disturbances are accounted for —, this problem allows to easily assess the outcome of both the control and integrated design processes.

Both CVPs introduced in Section 2.3 are exercised for the optimal control of the system and results are compared against Ref. [31]. In order to show the effect of using different discretisations and problem formulations, the behaviour of two pendula of different flexibility is analysed (Section 3.2). The impact of the actuation bandwidth and the structural nonlinearities is further assessed in Section 3.3. Finally, a multi-resolution strategy is proposed to improve the convergence characteristics of the process (Section 3.4).

3.1. Problem description

The flexible pendulum configuration proposed in Ref. [31] is sketched in Fig. 2. The pendulum is modelled as a hinged elastic beam and lies initially in a stable equilibrium position along the vertical direction (Z-axis), gravity effects being accounted for. In order to control the system, an actuating torque, $M_Y(t)$, chosen to be zero at the initial and final time of the simulation, is applied at its root (Fig. 2), causing the pendulum to oscillate about the hinge point. The torque time history $M_Y(t)$, in particular, is optimised such as to maximise the leftward X velocity of the pendulum tip, v_X, measured in the global FoR at time $T = 2$ s. The problem is fully deterministic and any sources of friction or damping are not considered.

[1] From Fourier's theorem any signal u defined over the domain $[0, T]$ can be reproduced by a large enough sine series.

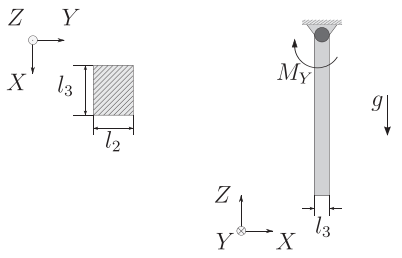

Fig. 2. Flexible pendulum geometry.

To account for the cost of actuation, Wang and Yu [31] augmented the cost function with the quadratic force regulator term

$$P[M_Y] = \frac{1}{2}\int_0^T \left[\pi_1\, M_Y^2 + \pi_2 \left(\frac{\mathrm{d}M_Y}{\mathrm{d}t}\right)^2\right] \mathrm{dt} \tag{11}$$

which depends on both the magnitude and the rate of change of the actuation. The optimal control problem can thus be written, in its continuous form, as:

$$\begin{aligned} \text{min.} \quad & I = \kappa_1\, v_X(T) + \kappa_2\, P \\ \text{w.r.t.} \quad & M_Y(t) \\ \text{s.t.} \quad & M_Y(0) = M_Y(T) = 0 \\ & -M_{\max}(t) < M_Y(t) < M_{\max}(t) \end{aligned} \tag{12}$$

where I is the augmented cost function and the constants κ_i and π_i are scaling parameters to ensure that all the terms in the cost function and the force regulator equations have same units and comparable magnitude; note, in particular, that κ_1 is required to have negative value. In the following, we will refer to problem (12) as the augmented problem. In the numerical implementation, M_Y is discretised by means of DS (Eq. (8)) and B-spline (Eqs. (9), (10)) basis functions; the optimisation is thus performed with respect to the coefficients of the parametrisation, x_c.

The augmented problem (12) defines a trade-off between performance (v_X term) and cost of actuation (P term). While this approach is in line with many practical control strategies (e.g. LQR feedback controllers), it can also affect the convexity of the design space and lead to path dependent solutions in the optimisation process. Therefore, the optimal control problem has also been formulated in a constrained version:

$$\begin{aligned} \text{min.} \quad & v_X(T) \\ \text{w.r.t.} \quad & M_Y(t) \\ \text{s.t.} \quad & P \le P_{\max} \\ & M_Y(0) = M_Y(T) = 0 \\ & -M_{\max}(t) < M_Y(t) < M_{\max}(t) \end{aligned} \tag{13}$$

The integral term P acts as a measure for the energy that the actuation can transfer into the dynamical system. Constraining this quantity allows, therefore, to bound the level of kinematic displacements displayed by the structure and, consequently, the amount of nonlinear effects experienced of the system. As it will be shown in Section 3.3, this has a significant impact on the design space smoothness.

3.2. Optimal control results

The optimal control problem for the flexible pendulum (Fig. 2) is initially solved using the augmented formulation defined in problem (12) and results are compared to those obtained by Wang and Yu [31]. The pendulum is modelled as a beam of constant rectangular cross-section with area $A = 10^{-2}$ m^2 and negligible rotational inertia; an isotropic material of Young's module $E = 1.2$ Pa and density $\rho = 100$ kg m^{-3} was used to reproduce the inertia and stiffness properties in Ref. [31]. The actuation was bounded not to exceed absolute value of $M_{\max} = 3.5$ N m, while cost and penalty term parameters appearing in problem (12) were set as per Ref. [31] to be

$$\kappa_1 = -1 \text{ s m}^{-1}, \quad \kappa_2 = 1$$
$$\pi_1 = 1 \text{ N}^{-2} \text{ m}^{-2} \text{ s}^{-1}, \quad \pi_2 = 10^{-2} \text{ N}^{-2} \text{ m}^{-2} \text{ s}$$

Since rigid body rotations and deformations are all planar, the only relevant elastic quantity is the bending stiffness in the plane of motion. Two beams, one being 10 times stiffer than the other, are obtained varying the sides of the cross-section l_2 and l_3 while keeping the sectional area. They are referred to as *stiff* and *flexible* pendulum in Table 1.

The characteristic frequencies in Table 1 have been computed around the underformed pendulum configuration to give an idea of where the resonance points are located in the nonlinear structure. Note that, as the structure becomes more

Table 1
Pendula structural properties for the optimal control problem.

Case	l_2 (m)	l_3 (m)	EI (N m^2)	f_r (Hz)	f_b (Hz)
stiff pendulum	0.1000	0.1000	10.0	0.50	7.76
flexible pendulum	0.3162	0.0316	1.0	0.50	2.45

Table 2
Optimal control results of the *stiff* pendulum using different parametrisations.

Parametrisation	N_c	$f_{\max}$ (Hz)	N_I	$v_X(T)$ (m s^{-1})	P	I
spline	11	2	20	6.08	2.73	−3.35
DS	8	2	14	6.08	2.73	−3.35
spline	43	10	33	12.35	6.18	−6.17
DS	40	10	44	10.57	4.77	−5.80

flexible, the natural frequency related to the first bending mode f_b drops and the coupling between flexible and rigid body dynamics increases.

For both cases proposed in Table 1 the optimal control problem is solved with B-spline and DSS parametrisations of different basis sizes, based on the maximum frequency, $f_{\max}$, captured by the control. However, fixed a certain value of $f_{\max}$, the size of DSS and B-spline basis are comparable (Section 2.3). In particular, for each parametrisation the basis size was chosen such as to exclude ($f_{\max} < f_b$, low bandwidth control) and include ($f_{\max} > f_b$, high bandwidth control) the flexible mode natural frequency of vibration. It should be finally noted that the range of frequencies of interest falls within the domain of simple optical recognition methods [32], making this set-up suitable for experimental verification.

3.2.1. *Stiff pendulum*

The *stiff* pendulum will be subject to the control actions in Table 2. In the table, N_c and $f_{\max}$ refer to the basis size of each parametrisation and the related maximum frequency of actuation, respectively. Optimal control results are presented in terms of cost (I), penalty factor (P) and final pendulum tip velocity, $v_X(T)$. N_I is the number of iterations required to complete the optimisations.

When using $f_{\max} = 2$ Hz, the optimal actuation does not excite the first bending mode of the pendulum, which, therefore, mostly swings rigidly. This can be observed in Fig. 3, where the snapshots of the actuated pendulum position, driven by the DSS modelled optimal torque, show no relevant elastic deformation. Comparing optimal actuation and tip displacements time histories against Ref. [31] demonstrates that both the spline and DSS parametrisation can capture well the rigid-body motion frequency (Fig. 4), thus returning very similar performances (Table 2). As physically expected, the control moment, M_Y, excites the rigid-body motion only and uses the gravity potential energy to increase the final tip velocity, $v_X(T)$, while limiting the overall actuation cost, P.

Setting $f_{\max} > f_b$ leads to a large increase of the final tip velocity, $v_X(T)$, as the first bending mode is excited (Fig. 5). The active system is now capable of storing elastic energy, which is converted into kinetic energy as $t \to T$, providing a further contribution to v_X and enhancing the overall system performance. With both splines and DSS, the high frequency component is larger than in the solution obtained by Wang and Yu [31]. It has to be noticed, however, that results in Ref. [31] are obtained from optimisations that are stopped after only 10 iterations and a beam model that includes structural damping. This likely explains the small differences between both sets of results.

While the optimal actuation always shows to correctly exploit the system physics, the 10 Hz bandwidth solutions obtained with the two parametrisations point towards two different minima, corresponding to two different levels of control actuation, P. To verify the existence of local minima, the control design space has been sampled for a case in which the pendulum is actuated by a control parametrised with only two sine waves. To model a low bandwidth actuation, these were chosen to have frequencies 0.5 Hz and 0.75 Hz, with amplitudes $x_{0.5}$ and $x_{0.75}$, respectively. These are associated to a left/right and left/right/left rigid-body mode and, as physically expected, had been observed to have a large contribution in both the 2 Hz and 10 Hz DSS parametrised optimal actuations.

The contour lines of the cost I, obtained when varying the amplitude of the two sine waves, are shown in Fig. 6a, together with the isolines of the force regulator term, P (thick curves). The design space is smooth with a minimum at $(x_{0.5}, x_{0.75}) = (0.88, 1.83)$ N m. Despite the reduced size of the parametrisation, cost and penalty at the minimum ($I = -2.94$ and $P = 2.46$) compare well with those obtained using a low bandwidth actuation ($f_{\max} = 2$ Hz in Table 2).

To model a high bandwidth control, the amplitude $x_{0.75}$ of the 0.75 Hz sine wave was fixed to be 1.7 N m and a high frequency sine wave (7.75 Hz, near the first natural frequency) of amplitude $x_{7.75}$ was added to the parametrisation. As before, both coefficients of the parametrisation were varied so as to reconstruct the cost function I over the control design space (Fig. 6b). While a minimum — corresponding to a predominantly low-frequency actuation that only exploits the rigid-body dynamics — is

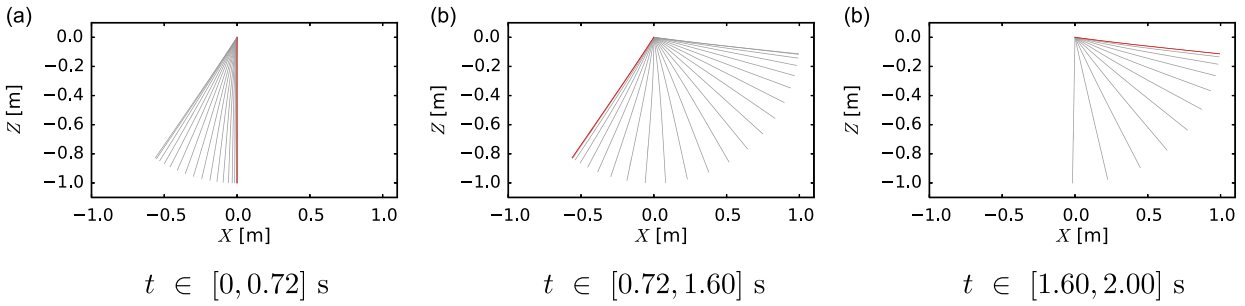

Fig. 3. Snapshots (25 frames per second) of the *stiff* pendulum response for the optimal actuation with a control maximum frequency $f_{\max} = 2$ Hz using a DSS parametrisation. (A thick line identifies the initial shape).

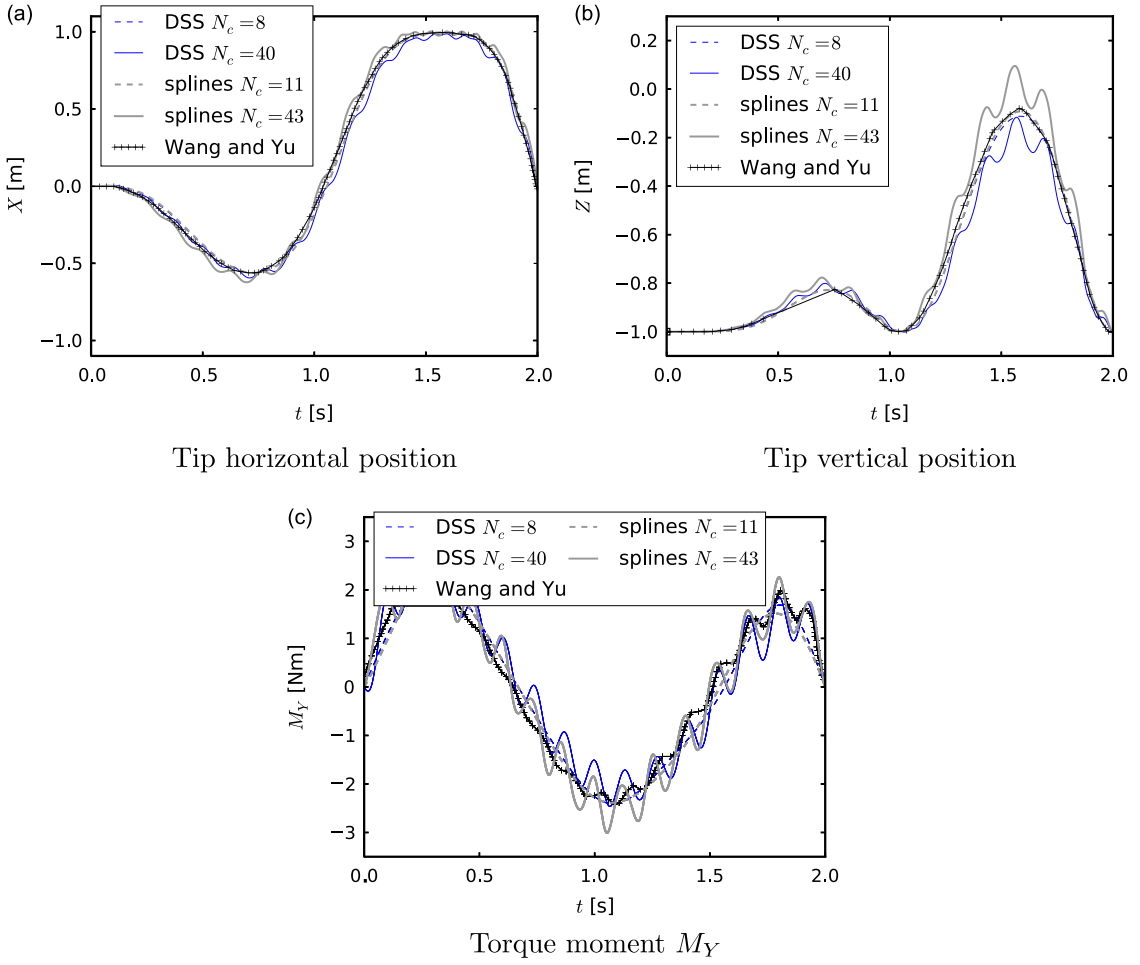

Fig. 4. Time histories under optimal control of the *stiff* pendulum using different parametrisations of the torque signal.

still observed for $x_{7.75} \approx 0$, a new minimum, corresponding to a peak of structural resonance, appears. A further investigation on how both minima change with the amplitude and frequency of the excitation is included in Section 4.1.

Sampling the cost function I has therefore shown that when the control can exploit resonances, multiple minima can populate the design space. The reason why the high bandwidth actuations provided by splines and DSS lead to distinct point of minimum can then be linked to how different sets of basis functions reconstruct the actuation. While a control signal parametrised with a low number of spline basis cannot be built for direct comparison with Fig. 6b, it is clear that as the mapping between parametrisation coefficients x_c and final cost I changes, so does the location of the minima.

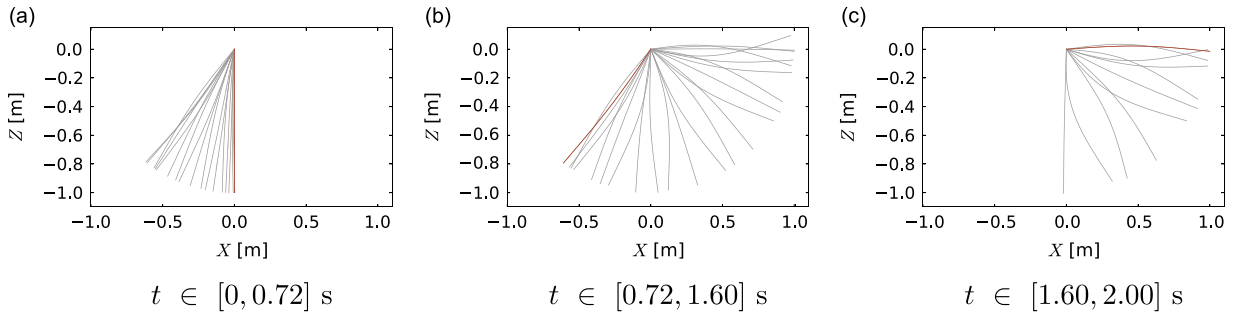

Fig. 5. Snapshots (25 fps) of the *stiff* pendulum response for the optimal actuation obtained using a B-spline parametrisation with $N_c=43$ control points ($f_{\max}=10$ Hz). A thick line identifies the initial shape.

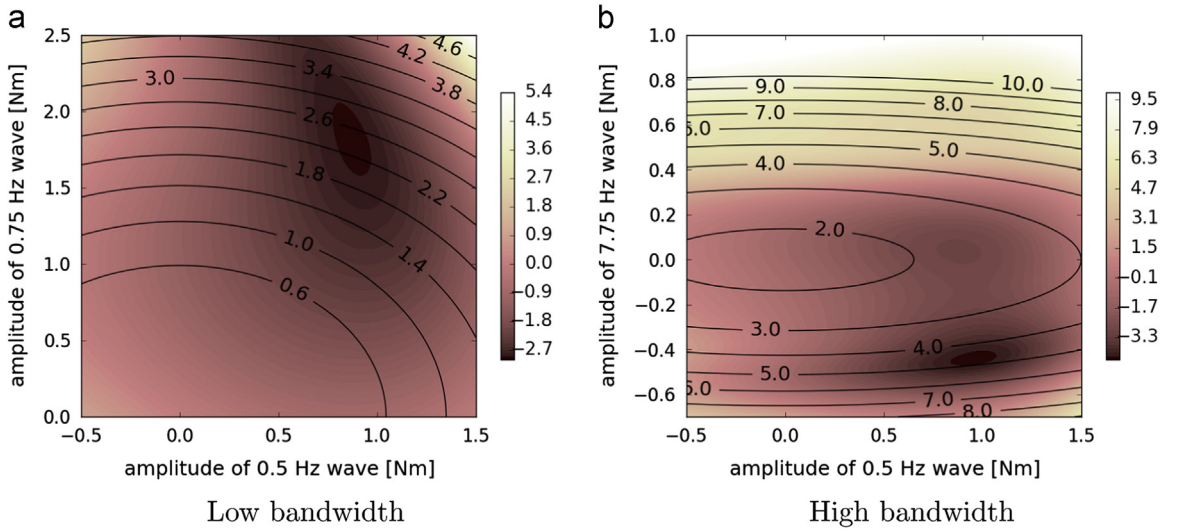

Fig. 6. Cost function, I, associated to a *rigid* pendulum when varying the amplitude of the sine waves parametrising the actuating torque, M_Y.

3.2.2. *Flexible pendulum*

The study of the low-bandwidth actuated *stiff* pendulum has shown that, when the actuation can only excite the rigid-body mode of vibration, the design space is smooth and the actuations provided by splines and DSS parametrisations are in good agreement. As the pendulum flexibility is increased, however, the distance between rigid and flexible body characteristic frequencies, f_r and f_b, is drastically reduced (Table 1) and it becomes harder to excite one of the modes without exciting the other.

The implications of an increasing rigid-flexible body dynamics coupling are highlighted by the results obtained using DSS and spline basis to parametrise two low-bandwidth actuations ($f_{\max}<f_b$) having $f_{\max}=1.25$ Hz and a $f_{\max}=1.5$ Hz. The optimal torque time histories (Fig. 8a) and the associated cost, I, and penalty factor, P, compare well across parametrisations only when $f_{\max}=1.25$ Hz (Table 3). However, as clearly shown by the snapshots in Fig. 7, the DSS modelled actuation with $f_{\max}=1.5$ Hz can excite the pendulum bending mode, allowing to reach a cost 22 percent lower than when using a splines parametrisation. This is verified in Fig. 8b, where the DS decomposition of the optimal actuations are shown.[2] While for the $f_{\max}=1.25$ Hz cases these can only excite the rigid-body dynamics, raising $f_{\max}$ allows the control to mildly excite the pendulum bending mode. The different resolution between the parametrisation becomes, at this point, critical: the DSS basis can express a strong frequency content around $f_{\max}=1.5$ Hz, whereas this cannot be achieved using splines. The more aggressive control obtained using DSS (note that the force regulator term P almost doubles with respect to the corresponding spline case) is, therefore, justified by the different resolution.

As seen in Fig. 9, when using a higher bandwidth control ($f_{\max}>f_b$), both discretisations capture well the very flexible beam dynamics. However, and as already discussed for the *rigid* pendulum in Section 3.2.1, the dynamics under resonance increases the path dependency of the results. This can be seen in Fig. 8c and d: while the final cost, I, compares well across

[2] The DS expansion of a general signal u defined over a domain $[0,T]$ can be obtained by applying a Fourier transform to the extended signal $\tilde{u}=\begin{cases}\tilde{u}=u(t), & t\in[0,T]\\ \tilde{u}=-u(-t+2T), & t\in[T,2T]\end{cases}$ defined over the domain $[0,2\ T]$.

Table 3
Optimal control results of the *flexible* pendulum using different parametrisations.

Parametrisation	N_c	$f_{\max}$ (Hz)	N_I	$v_X(T)$ (m s^{-1})	P	I
spline	8	1.25	29	4.63	1.59	−3.04
DS	5	1.25	16	4.48	1.59	−2.89
spline	9	1.5	22	5.40	2.19	−3.21
DS	6	1.5	40	8.42	4.50	−3.92
spline	19	4	57	15.92	5.73	−10.19
DS	16	4	53	13.11	3.48	−9.63

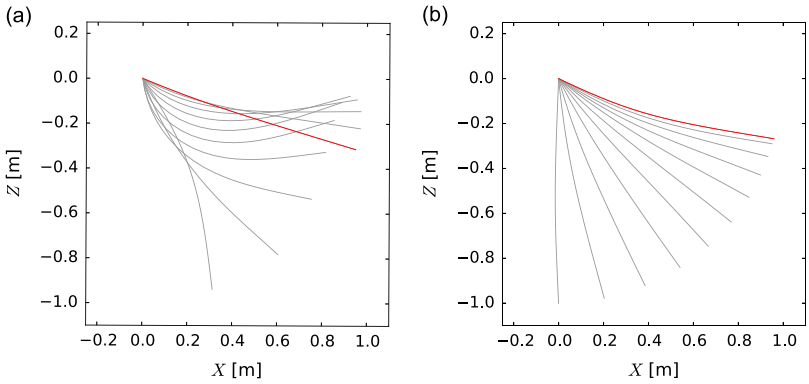

Fig. 7. Snapshots (25 fps) of the *flexible* pendulum response for $t \in [1.60, 2.00]$ s with optimal control parametrisation having a maximum frequency $f_{\max} = 1.5$ Hz. (A thick line identifies the initial shape).

parametrisations, the splines obtained solution has now a considerably more aggressive actuation (Table 3). Results also include those of Ref. [31], which account for damping in the model and, as before, show a smoother behaviour.

3.2.3. *Path dependency vs. problem formulation*

When dealing with resonance conditions the optimal actuation torque, M_Y, obtained from the augmented problem (12), was found to be parametrisation dependent. The control of the *flexible* pendulum has also underlined that the parametrisation resolution can also have an effect, especially when dealing with an increasing coupling between flexible and rigid body dynamics. To isolate the impact of the problem formulation from that of the parametrisation (which will be the focus of Section 3.3), the optimal control of the *stiff* and *flexible* pendulum is obtained now using the constrained formulation (13). Large deformations are still allowed due to a large maximum actuation ($P_{\max} = 6$) and a high bandwidth ($f_{\max} > f_b$). The results are shown in Table 4 and present a much higher consistency in the optimal control across both discretisations. Having removed the penalty term from the cost function definition, the optimal actuation always reaches, as expected, the limit $P_{\max} = 6$. For the *stiff* pendulum case, the two parametrisations are in extremely good agreement. As the system becomes more nonlinear (*flexible* pendulum), however, spline basis seem to be able to better capture the system resonance, leading to a 1.9 percent higher tip velocity $v_X(T)$.

Fig. 10 shows however that better performance of the spline is not linked to better reconstruction properties. Converting the spline parametrised optimal actuation in a DSS shows, in fact, that this has no relevant frequency content over $f_{\max} = 4$ Hz (Fig. 10a). In fact, the spline optimal actuation is reconstructed using a DSS series in Fig. 10b. Applying the reconstructed torque to the pendulum, a final tip velocity $v_X(T) = 15.62$ m s^{-1}, which is in line with the performance provided by the spline optimal actuation, is achieved.

It can thus be concluded that, despite the use of a *constrained* problem formulation, the two parametrisations can still converge to different minima as the nonlinearity of the system increases. While results are in very good agreement for the *stiff* pendulum, the DSS actuation leads to a control with a higher low frequencies for the *flexible* pendulum case (Fig. 10a). The use of a *constrained* problem formulation, however, reduces the gap between the two solutions, as the level of actuation, $P_{\max}$ — and consequently the final tip velocity, $v_X(T)$ — are now comparable. This formulation, which diverges from that of [31], has been therefore chosen to further investigate the impact of both frequency resolution and level of actuation in the next section.

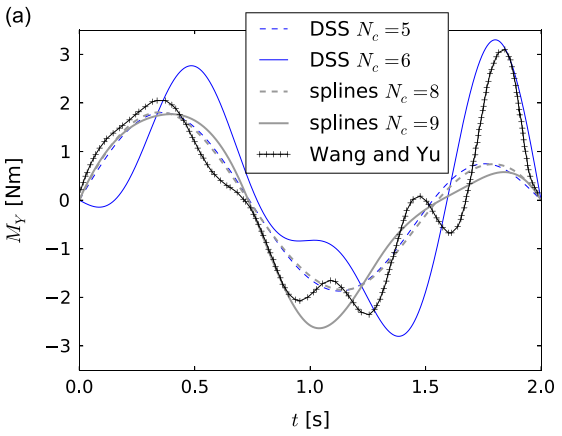

Low-bandwidth torque moment M_Y

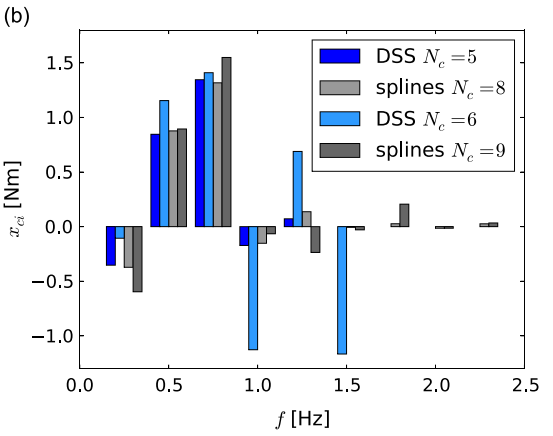

DS comparison between low-bandwidth optimal actuations ($f_{max} = 1.25$ Hz and $f_{max} = 1.5$ Hz)

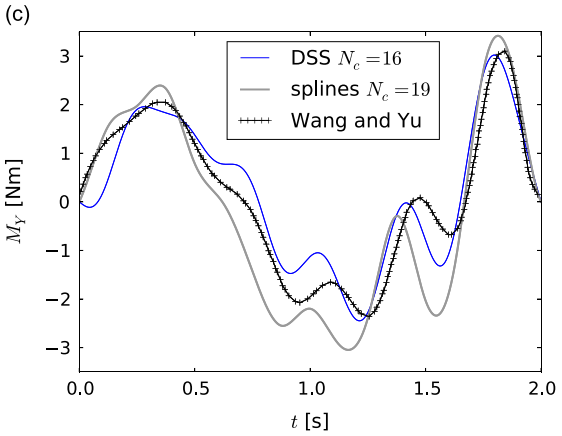

High-bandwidth torque moment M_Y

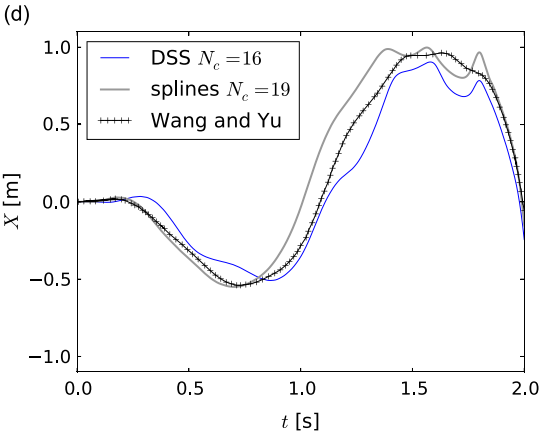

Tip horizontal position under high-bandwidth actuation

Fig. 8. Time histories under optimal control of the *flexible* pendulum using different parametrisations of the torque signal.

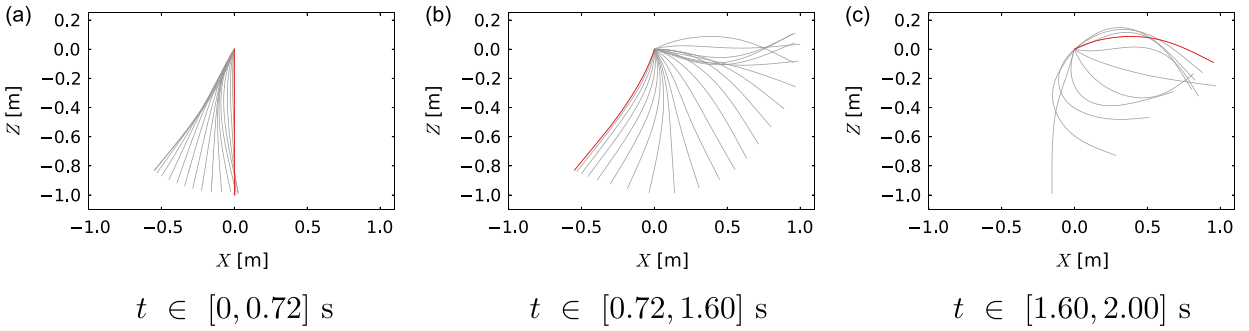

Fig. 9. Snapshots (25 fps) of the *flexible* pendulum response for the optimal actuation obtained using a B-spline parametrisation with $N_c = 19$ control points ($f_{\max} = 4$ Hz). A thick line identifies the initial shape.

3.3. Parametrisation vs. system nonlinearity

In order to investigate further the duality between local and global parametrisations, the optimal control problem of the pendulum is solved using both B-splines and DSS for a range of beams of different stiffness. In both cases the number of basis functions is chosen such as to achieve a maximum frequency $f_{\max} = 6$ Hz. The pendulum bending stiffness is varied by

Table 4
Optimal control results for the *stiff* and *flexible* pendulum using the constrained formulation (13) and setting $P_{\max}=6$.

Pendulum	Basis	$f_{\max}$ (Hz)	N_l	$v_X(T)$ (m s^{-1})	P
stiff	spline	10	40	12.30	6.00
stiff	DS	10	170	12.27	6.06
flexible	spline	4	54	15.73	6.00
flexible	DS	4	158	15.43	5.96

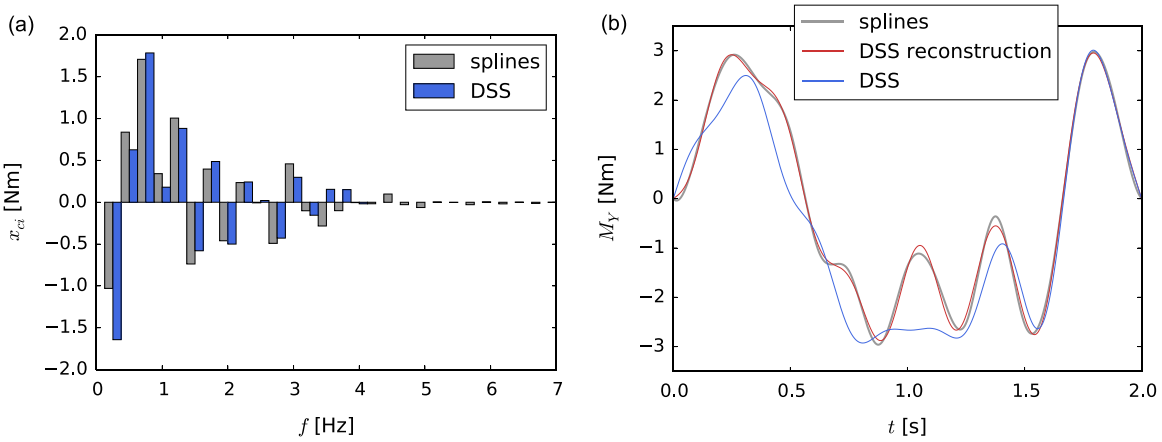

DSs comparison between optimal actuations

Torque comparison and reconstruction of spline optimal actuation via DSS

Fig. 10. Comparison between spline and DSS optimal actuation for *flexible* pendulum case and no penalty factor.

changing the aspect ratio of the beam cross section (Fig. 2) under constant sectional area, $A=10^{-2}$ m. As a result, the rigid-body mode natural frequency, f_r, remains unaltered.

Varying l_3 between $[0.05, 0.10]$ m resulted in a design space including situations for which the chosen maximum control frequency is either greater or smaller than the pendulum first bending natural frequency, f_b. More specifically, f_b has values between 3.88 Hz and 7.76 Hz and it is $f_b=f_{\max}$ when EI$=5.98$ N m^2 and $l_3=0.0773$ m. The lower bound for the beam stiffness is such that the resonance of the second bending mode is avoided. While this could also be exploited, it was not included in this exploratory study to simplify the analysis.

The constrained optimisation problem (13) is solved for three levels of admissible actuation ($P_{\max}=2,4,6$) to assess the impact of increasing nonlinear effects on the solution. Results are shown in Fig. 11. The design space can be divided into three regions according to whether the control can or cannot excite the pendulum bending mode. When the bending natural frequency, f_b, is well below the maximum frequency of actuation $f_{\max}$ ($l_3 \lessapprox 0.070$ m), the control signal can excite the rigid-flexible body dynamics, providing high performance. In this situation, in fact, the actuation has a high bandwidth in relation to the physical properties of the system ($f_{\max} \gg f_b$). When $l_3 \gtrapprox 0.085$ m, on the other hand, the same control with $f_{\max}=6$ Hz has now a low bandwidth. As a result, only the rigid body dynamics is exploited and performance decreases. At last, a transition region ($0.070\text{ m} \lessapprox l_3 \lessapprox 0.085$ m), in which resonance outsets, can be identified.

The classification introduced can be more clearly understood by looking at Fig. 12, where the magnitude ($|x_{cn}|$ in Eq. (7)) of the basis functions of the DSS parametrised optimal control is shown for a range of different pendula stiffness and actuation cost, $P_{\max}$. As it can be seen, the control effort is concentrated in two regions, the first one located in the low frequency range so as to excite the rigid body dynamics. The second one is observed when f_b is in the control range: a peak around this frequency appears and, as the beam stiffness varies, this moves to follow the bending mode natural frequency. Increasing the level of actuation, $P_{\max}$, larger geometrical deformations appear and resonance intensifies. The consequently higher level on nonlinearities in the problem is clearly reflected in the design space smoothness, which is visibly reduced when passing from $P_{\max}=2$ (Fig. 12a) to $P_{\max}=6$ (Fig. 12c).

Under low frequency actuation ($f_{\max} \ll f_b$), spline basis can achieve slightly better performance because their spectrum extends above $f_{\max}=6$ Hz, allowing the torque to mildly excite the pendulum bending mode. The phenomenon is consistently stronger for larger values of actuations.

As expected, the transition region ($0.070\text{ m} \lessapprox l_3 \lessapprox 0.085$ m) sees a change in performance due to the switch from rigid-flexible to rigid body only dynamics. The difference increases with $P_{\max}$, as stronger actuations induce a more intense level of resonance. The change in maximum tip velocity, $v_X(T)$, is sharper when using a DSS, whose related optimal control generally provide higher performance than the spline one. Contrarily to what it was seen in Section 3.2.3, however, this is

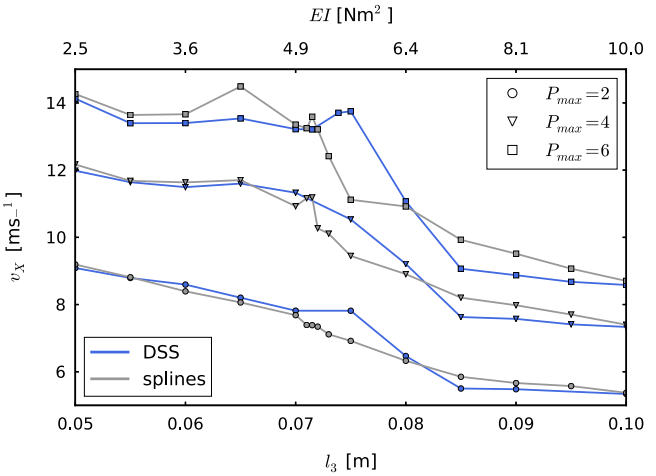

Fig. 11. Final tip velocity, $v_X(T)$, obtained using different parametrisations and levels of actuation $P_{\max}$.

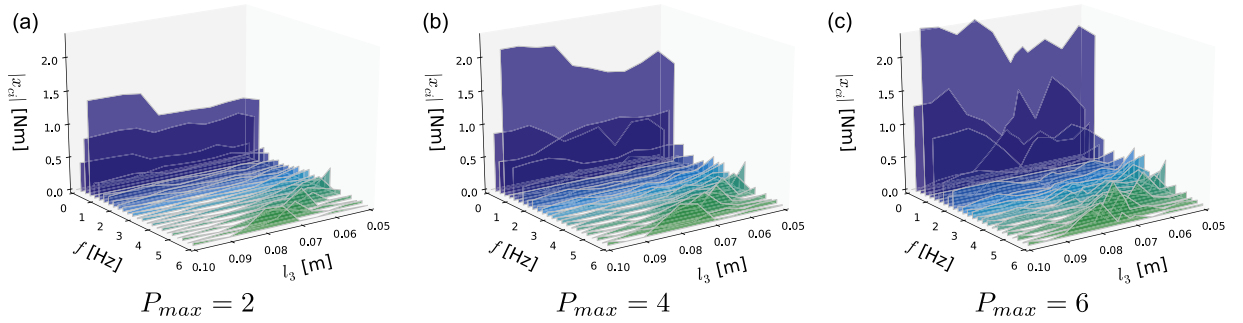

Fig. 12. Optimal actuation frequency content ($|x_{ci}|$) using a DSS parametrisation ($f_{\max}=6$ Hz) and a constrained problem formulation (13). Different levels of actuation, $P_{\max}$, are allowed.

not linked to the DSS providing better convergence properties but to the fact that in the transition region the solution quality is dictated by the parametrisation frequency content.

This is finally demonstrated in Fig. 13, where the optimal actuations provided by the two parametrisations for the case $l_3=0.0750$ m and $P_{\max}=4$ are compared. The DSS representation of the two signals (Fig. 13a) shows that the DSS parametrised control has a higher frequency content around the bending natural frequency, $f_b=5.63$ Hz: this allows to better excite the mode and achieve a larger final tip velocity, $v_X(T)$. As observed in Fig. 13b, however, the optimal actuation obtained using a DSS cannot be reproduced using B-splines. As a result, in the transition region DSS outperforms B-splines as it can better excite higher frequencies.

3.4. A multi-resolution strategy

Finally, a multi-resolution approach is proposed to improve optimisation convergence when strong structural nonlinearities are present. Fig. 11 has shown that for high frequency actuations and mild level of nonlinearity ($P_{\max}=2,4$), results compare well across different parametrisations. Both DSS and B-splines capture accurately the relevant high frequencies necessary to induce the system resonance. When the level of actuation is increased ($P_{\max}=6$), peaks of resonance become more evident as a consequence of larger displacements. These tend to arise whenever the bending oscillation period is a divisor of the time horizon T. While the location of the peaks is well captured by both basis, their amplitude can become parametrisation dependent. In fact, around the peaks of resonance there are large changes in performance for small variations in the actuation. There local basis tend to perform better, as they scale more efficiently. During the sensitivity analysis, in fact, a variation applied to one of the basis functions only affects a portion of the domain, leading to an overall smaller perturbation of the original signal. For the same reason, when updating the actuation, changes in torque signal tend to be more contained than when using a DSS. As a consequence, smaller steps between one design point and another are taken by the optimiser. This facilitates the reconstruction of the design space around the peak regions, despite the high sensitivity of the cost function to variations of the design.

A multi-resolution strategy can be used to accelerate convergence on those situations. The optimal control problem is hierarchically solved for parametrisations of increasingly higher bandwidth. The method is demonstrated here for the case of a

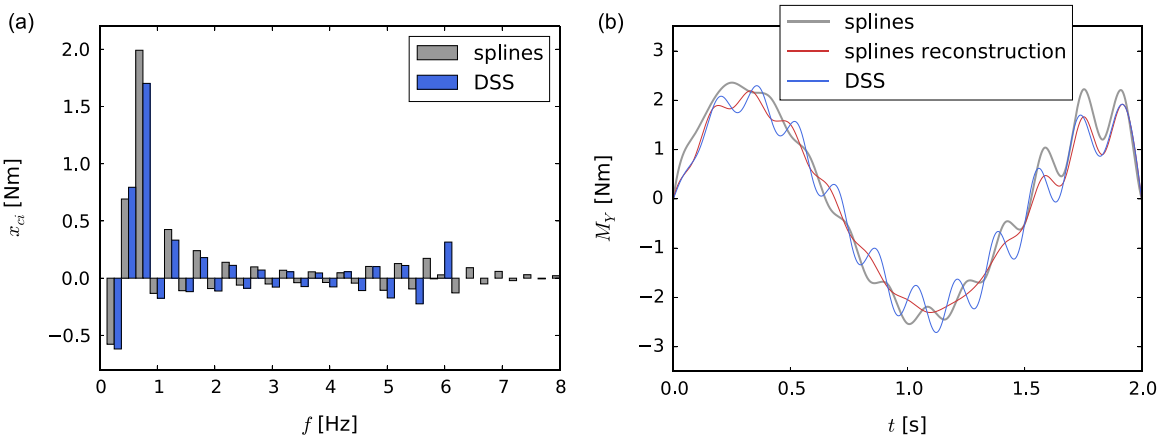

DSS optimal coefficient against DS representation of spline solution

Time histories and spline reconstruction of DSS optimal actuation

Fig. 13. Optimal actuation in the transition region ($l_3 = 0.0750$ m and $P_{\max} = 4$) using different parametrisations.

Table 5
Optimal control results at different stages of a multi-resolution based process using a DSS parametrised actuation ($f_{\max} = 12$ Hz).

Stage	N_c	$f_{\max}$ (Hz)	$v_X(T)$ (m s^{-1})	P
1	24	6	10.71	6.004
2	32	8	13.41	6.004
3	40	10	13.51	6.038
4	48	12	13.54	6.051
direct	48	12	12.22	6.019

pendulum of bending stiffness EI$=6.4$ N m^2 and whose actuation is obtained through a large bandwidth DSS parametrisation ($f_{\max} = 12$ Hz). The steps of the process are summarised in Table 5, where the results obtained without applying a multi-resolution strategy are also reported (*direct* label). Initially, the actuation bandwidth is set to 6 Hz. Once an optimal actuation is found, this is increased by 2 Hz so as to refine the torque time history; the procedure is repeated until $f_{\max} = 12$ Hz.

As expected, the pendulum final tip velocity, $v_X(T)$, is drastically increased at the second stage of the process, as the actuation bandwidth becomes larger than the pendulum bending mode natural frequency ($f_b = 6.21$ Hz). Further increments to the maximum actuation frequency, $f_{\max}$, however, do not lead to any relevant change in $v_X(T)$: contrarily, as the parametrisation becomes over-resolved ($f_{\max} \gg f_b$) the convergence of the optimisation process is compromised and the constraint $P \leq 6$ is not fully recovered. The link between over-resolution and convergence slowdown is even more clear when looking at the results obtained without multi-resolution analysis. In this case, not only the constraint $P \leq 6$ is not fully recovered, but also the final actuation time history shows to be not fully converged, as $v_X(T)$ achieved is 8.9 percent lower than the one provided by the multi-resolution approach.

4. Numerical studies on active system co-design

The same flexible pendulum test case of Section 3 is used now to test the co-design approach presented in Section 2.2. As the pendulum bending stiffness has been shown to be the most relevant structural property to impact the system dynamics, it will be allowed to vary while the actuation itself is being defined. The effect of choosing a different starting condition for the actuation, as well as the potential disadvantages of using a sequential approach, is investigated in Section 4.1. Section 4.2 focuses on the efficiency of the process, showing how the convergence speed can be affected near resonance and how to tackle the issue. Finally, the impact of the frequency resolution chosen to model the actuation is discussed in Section 4.3.

For all the co-design cases considered in this section, the beam rectangular cross-section (Fig. 2) is initially set to have a relatively high bending stiffness, EI$=6.4$ N m^2, and size $l_2 \times l_3 = 0.080 \times 0.125$ m^2. During the co-design, l_3 has been bounded to be $l_3 \in [0.055\text{ m}, 0.200\text{ m}]$, while l_2 is constrained as before to maintain the beam cross-sectional area constant ($A = 10^{-2}$ m^2). As the bending mode natural frequency of the initial design is $f_b = 6.21$ Hz, the basis size of the parametrisation has been adjusted so as to reach a maximum frequency $f_{\max}$ equal to 4 Hz, 6 Hz (as per the design of experiment in Fig. 11) and 12 Hz. The optimisation has been formulated as the constrained problem (13) with $P_{\max} = 6$. This allows to test the co-design process for a highly nonlinear configuration while reducing the path dependency of the solution.

Table 6
Results of the combined optimisation problem using DSS control parametrisations of different basis size. Percentage values are with respect to the optimal control only case (DOE).

ID	N_c	$f_{\max}$ (Hz)	l_3 (m)	f_b (Hz)	$v_X(T)$ (m s^{-1})	%
zero	16	4	0.0550	4.27	10.61	33.5
zero	24	6	0.0739	5.73	13.70	28.0
zero	48	12	0.0792	6.15	13.34	−0.5
opt	16	4	0.0819	6.36	8.41	5.8
opt	24	6	0.0800	6.21	10.71	0.0
opt	48	12	0.0800	6.21	13.41	0.0
DOE	16	4	0.0800	6.21	7.95	–
DOE	24	6	0.0800	6.21	10.71	–
DOE	48	12	0.0800	6.21	13.41	–

The constraint on the sectional area maintains the inertial properties and thus the characteristic frequencies associated to the rigid-body dynamics of the different designs remain identical. To minimise the cost in problem (13), therefore, the co-design can only adjust the pendulum stiffness and tune its bending mode natural frequency with the frequencies content of the actuation. While a larger number of structural design parameters could be considered, a single parameter facilitates our exploration as it allows for a much clearer analysis of the results. Furthermore, dealing with nonlinear dynamics and a large number of structural design variables would require the development of an adjoint based sensitivity analysis, which is beyond the scope of this work.

The main results obtained of the co-design problem have been summarised in Tables 6 and 7. For each case, the size of the parametrisation, N_c, and the related maximum frequency of excitation, $f_{\max}$, have been reported. The identifications *zero* and *opt* refer to the torque time-history at the beginning of the optimisation process, M_{Y0}: For the *opt* cases, the initial design uses the actuation found in pure optimal control problem; for the *zero* cases, it is simply chosen to be $M_{Y0}(t)=0$ (*zero* cases). The optimal structural design is described both in terms of final geometry (l_3) and its bending mode natural frequency (f_b), while system performance is quantified by the final tip velocity, $v_X(T)$. This is compared to the tip velocity given by the optimal control problem on the initial beam geometry (DOE in the tables).

4.1. Initial condition: sequential vs. co-design

First, we will focus on the co-design results obtained when initialising the torque actuation with a previously computed pure optimal control solution (*opt* cases). This defines a situation similar to a sequential optimisation, and in fact, from Tables 6 and 7, it is clear that co-design brings almost no changes in either the structural design or in the actuation with respect to the initial design. This can also be observed by comparing the *DOE* and *opt* curves in Fig. 14, where the optimal actuations obtained with 4 Hz and 6 Hz bandwidth parametrisations are shown.

For the large bandwidth controls ($f_{\max}=6$ Hz, 12 Hz) this can be explained noticing that at the start of the optimisation the actuation M_{Y0}, which is the solution of an optimal control problem, can already excite the bending mode of the pendulum (note, for instance, the high frequency component in the *DOE* curve in Fig. 14a). As the process is initiated from a resonance condition, control force and the structural design are de facto *locked* into a local minimum. Further changes in the structure size would only lead to poorer performance, the system moving away from the resonance condition. Conversely, changes in the actuation signal would also imply moving away from resonance. As no descending direction can be found, the optimisation is interrupted after few iterations.

When the starting torque includes only lower frequencies ($f_{\max}=4$ Hz), the phenomenology that limits the performance improvements is similar. The initial excitation (see the *DOE* curve in Fig. 14b) exploits the rigid-body dynamics of the pendulum and, being far from resonance conditions, system performance can initially only be improved by stiffening the design, which ensures that all the energy transferred to the pendulum is stored by the rigid mode. Consequently, the co-design leads to a stiffer beam with only a small refinement on the actuation so as to better exploit the rigid-body dynamics of the system (see the *opt* curve in Fig. 14b).

The changes in the control design space leading to *locking* can be better understood with the reduced basis already introduced in Section 3.2.1. To reproduce a high-bandwidth actuation, the amplitude of the sine basis of frequencies 0.5 Hz ($x_{0.5}$) and 7.75 Hz ($x_{7.75}$) was varied, while the 0.75 Hz wave amplitude was fixed to 1.7 N m. The final tip velocity of the pendulum, $v_X(T)$, associated to different points $(x_{0.5}, x_{7.75})$ is shown in Fig. 15a. The isolines of the force regulator term P are also shown (black curves). Three high velocity regions, strongly dependent on the amplitude of the 7.75 Hz wave, are observed. For $P\leq 6$, the maximum velocity, $v_X(T)=9.36$ m s^{-1}, is found at point A $=(0.95, -0.49)$ N m. This is associated to a condition of resonance, as the bending mode natural frequency is $f_b=7.76$ Hz. As the initial structural design ($l_3=0.1$ m) is varied, the system moves away from the resonance. The high velocity regions initially move (Fig. 15b and c) and gradually smooth out (Fig. 15d and e). This shows that in the co-design space $(l_3, x_{0.5}, x_{7.75})$ a maximum is located around $l_3=0.1$ m, i.e. precisely where the bending mode natural frequency tunes with the actuation frequency of 7.75 Hz.

Table 7
Results of the combined optimisation problem using spline control parametrisations of different basis size. Percentage values are with respect to the optimal control only case (DOE).

ID	N_c	$f_{\max}$ (Hz)	l_3 (m)	f_b (Hz)	$v_X(T)$ (m s^{-1})	%
zero	19	4	0.0550	4.27	12.55	45.6
zero	27	6	0.0717	5.56	13.54	24.0
zero	51	12	0.0828	6.43	12.64	−9.2
opt	19	4	0.1465	11.4	8.65	0.3
opt	27	6	0.0800	6.21	10.92	0.0
opt	51	12	0.0800	6.21	13.71	0.0
DOE	19	4	0.0800	6.21	8.62	–
DOE	27	6	0.0800	6.21	10.92	–
DOE	51	12	0.0800	6.21	13.71	–

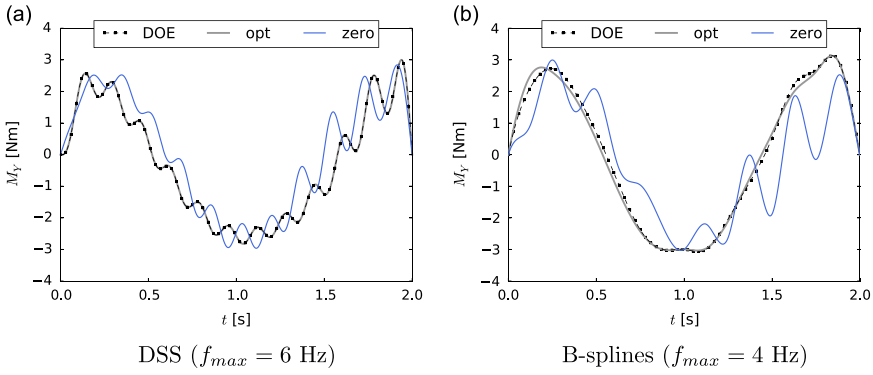

Fig. 14. Optimal actuation provided by the co-design using different starting conditions and parametrisations.

The mechanism determining the position of the high tip velocities regions in Fig. 15a is linked to the phase between the high frequency component of the actuation and the response of the pendulum in terms of its tip horizontal position. The global maximum (point A) is associated to the rigid-flexible body dynamics, while a second minimum, associated to predominantly rigid-body dynamics, is located at point B = (1.00, 0.063) N m. The actuation torque, M_Y, and the X tip position time histories of these cases are shown in Fig. 16 for $t \in [1.8, 2]$ s. As expected, for the actuation corresponding to point A, the high frequency component of M_Y synchronises with the displacements in such a way that, as $t \to T$, the tip velocity due to the structural vibration adds to the rigid-body rotation. Note that this is achieved for a negative amplitude of the 7.75 Hz wave, $x_{7.75}$. As expected, when $x_{7.75}$ increases and changes sign, the final tip velocity reduces because resonance provides a negative velocity increment. When, however, $x_{7.75} \gtrsim 0.5$ N m, $v_X(T)$ can be observed to grow again (Fig. 15a), meaning that the phase between actuation and pendulum tip response also depends on the actuation amplitude, $x_{7.75}$. This is also shown in Fig. 16, where the time histories of the actuation corresponding point C = (1.10, 0.98) N m in Fig. 15a are presented. This nonlinear effect is linked to the large rigid-body rotations of the pendulum and the changing geometric stiffness.

4.2. Robustness of the design

Contrarily to what it was observed in the previous section, when a null starting torque is used (*zero* cases in Tables 6 and 7), structural design and final system performance undergo a significant evolution. The outcome of the process largely depends in this case mostly on the control bandwidth. Generally, the co-design is driven towards a peak of resonance region, which, as it was already seen in Section 3.3, implies a slowdown of convergence, particularly for DSS parametrised controls. As a result, the optimiser typically does not recover the integral constraint $P \leq P_{\max}$. To overcome this, the following two-stage strategy was found to be an effective solution: once variations in the structural design are negligible, the pendulum geometry is fixed (end of first stage) and the actuation is refined by solving a pure optimal control problem (second stage). The improvements obtained by using the two-stage approach to refine the actuation are summarised in Table 8; as expected, the benefit is higher when the solution is closer to a peak of resonance.

The causes of the convergence slow down can be further investigated referring to the spline parametrised solution obtained with a 6 Hz bandwidth control. In this case, the optimiser correctly drives the structural design towards the peak region located around $l_3 = l_{\text{ref}} = 0.0715$ m (curve $P_{\max} = 6$ in Fig. 11). The neighbourhood of the peak of resonance is shown in more detail in Fig. 17. Here the coefficients of the optimal actuation x_c (Fig. 17b), and the resulting control signal (Fig. 17d), are compared

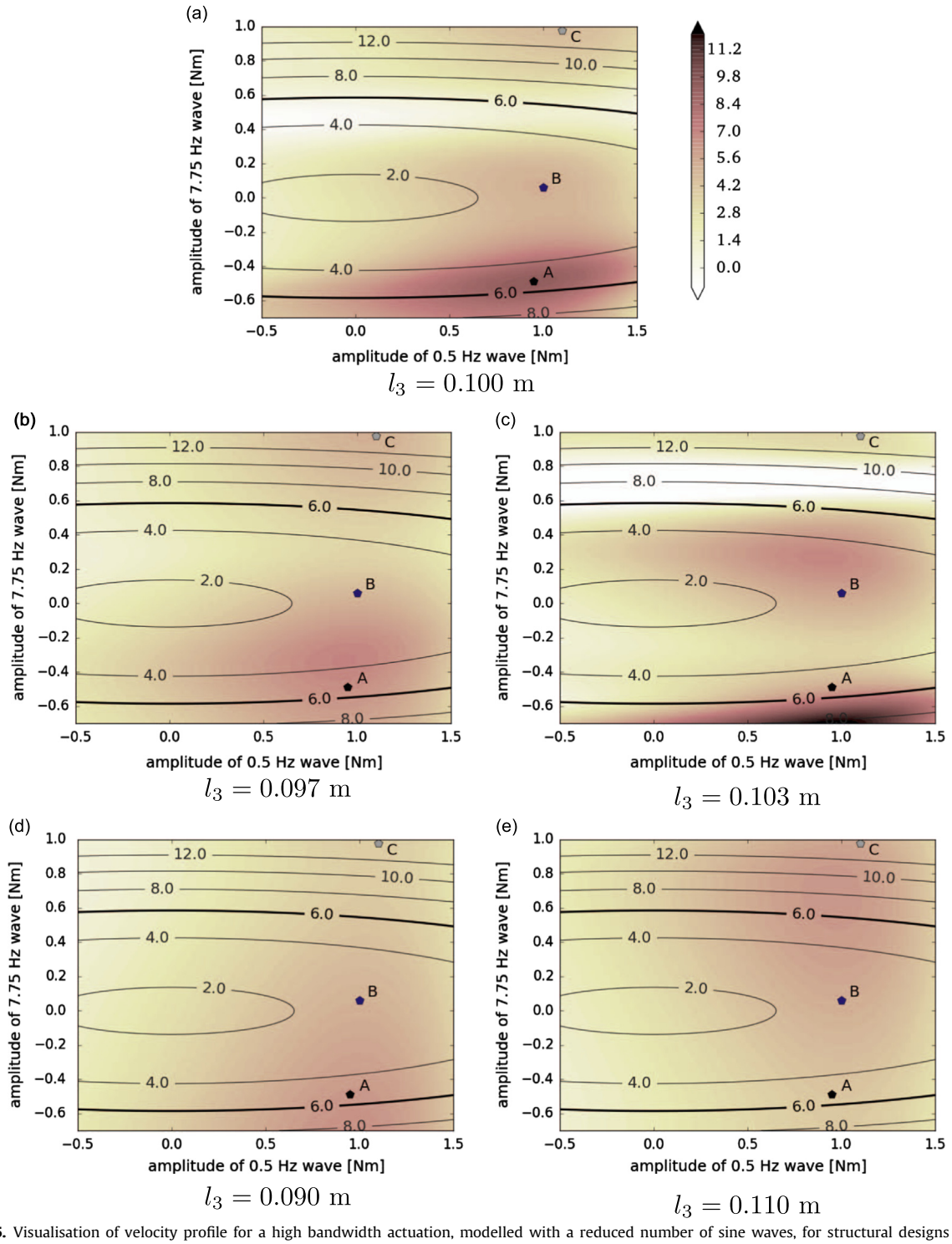

Fig. 15. Visualisation of velocity profile for a high bandwidth actuation, modelled with a reduced number of sine waves, for structural designs in the neighbourhood of $l_3 = 0.1$ m. Points *A*, *B* and *C* correspond to the coordinates of the local maxima found for $l_3 = 0.1$ m.

for structural designs in the vicinity of the peak of resonance. Despite the variations in the structure size being small,[3] $\Delta l_3 = \pm 0.007 l_{\text{ref}}$, the changes in the optimal actuation are, in proportion, considerably larger. This can be easily

[3] It is interesting to notice that, being the relation between l_3 and the bending mode natural frequency, f_b, linear, percentage variation in l_3 and f_b are equal.

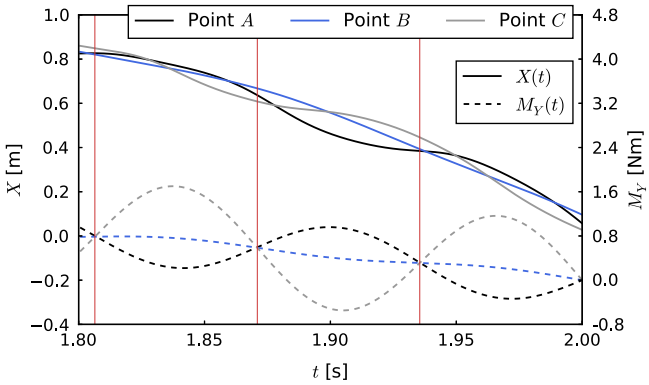

Fig. 16. Tip horizontal position and torque moment M_Y time histories of the *stiff* pendulum under the reduced DSS parametrised actuations corresponding to points A, B and C in Fig. 15a.

Table 8
Performance gains obtained using a two-stage co-design strategy.

Basis	$f_{\max}$ (Hz)	l_3 (m)	$v_X(T)$ (m s^{-1})		Gain %
			Not refined	Refined	
splines	4	0.0550	12.55	12.55	0.0
splines	6	0.0717	11.55	13.54	17.2
splines	12	0.0828	12.35	12.64	2.3
DSS	4	0.0550	10.50	10.61	1.0
DSS	6	0.0739	12.56	13.70	9.1
DSS	12	0.0792	11.72	13.34	13.8

observed by comparing Fig. 17b against Fig. 17a, where the optimal control coefficients around $l_3 = l_{\text{ref}} = 0.0715$ m, found enforcing a lower cost of actuation ($P_{\max} = 2$), are shown. Note that, in the latter case, nonlinear effects are significantly smaller.

The change in optimal actuation can be quantified by measuring the integral norm

$$\epsilon = \frac{\int_0^T (M_Y - M_{Y\text{ref}})^2 \, \mathrm{d}t}{\int_0^T M_{Y\text{ref}}^2 \, \mathrm{d}t} \tag{14}$$

where $M_{Y\text{ref}}$ and M_Y are the optimal actuations at the reference, $l_{\text{ref}} = 0.0715$ m, and the perturbed, $l_3 = l_{\text{ref}} \pm \Delta l_3$, design points (Fig. 17d). While perturbations in structural design are around 0.7 percent, the norm in Eq. (14) reaches values 16 times higher, being in both cases $\epsilon \approx 11$ percent. Large values of ϵ imply that, fixing the actuation and applying even a small change in the structural design, the system will tend to move far away from the optimal control condition. Not only, therefore, performance will decrease consistently, but, as discussed in Section 3.3, the parametrisation of the actuation will usually require a large number of iterations to adjust to the new structural design.

4.3. Impact of frequency resolution

From Tables 6 and 7, it can be observed that setting $M_{Y0}(t) = 0$ at the beginning of the co-design generally gives better performance, and that improvements are consistently larger when reducing the bandwidth of the control. When the highest bandwidth control is used ($f_{\max} = 12$ Hz), the actuation is capable of inducing resonance also on the initial design. Consequently, no major changes in the structural design occur, as this is driven towards the nearest peaks of resonance. The disadvantage of exploring a non-smooth region using a gradient based approach is shown by the fact that, while the DS parametrisation improves performance, with B-splines it degenerates and the solution converges towards a less resonant region.

Decreasing the actuation bandwidth, instead, leads to important performance increases with respect to the optimal control problem, regardless of the parametrisation used. The pendulum stiffness is, in fact, always reduced so as to drive its bending mode natural frequency towards the range on actuation of the control (note the f_b values in Tables 6 and 7). When $f_{\max} = 6$ Hz, the structural design is moved towards the peak of resonance located in the region $l_3 \in (0.070\text{ m}, 0.075\text{ m})$ and clearly visible from the design of experiment in Fig. 11. When $f_{\max} = 4$ Hz, the increase in flexibility is even larger and the lower bound of the structural design space, $l_3 = 0.0550$ m, is hit.

Especially in this case, the combined optimisation is shown to be capable of driving the structural design to a configuration where the initial control (with its limitations in terms of maximum frequency resolution) can now fully exploit the

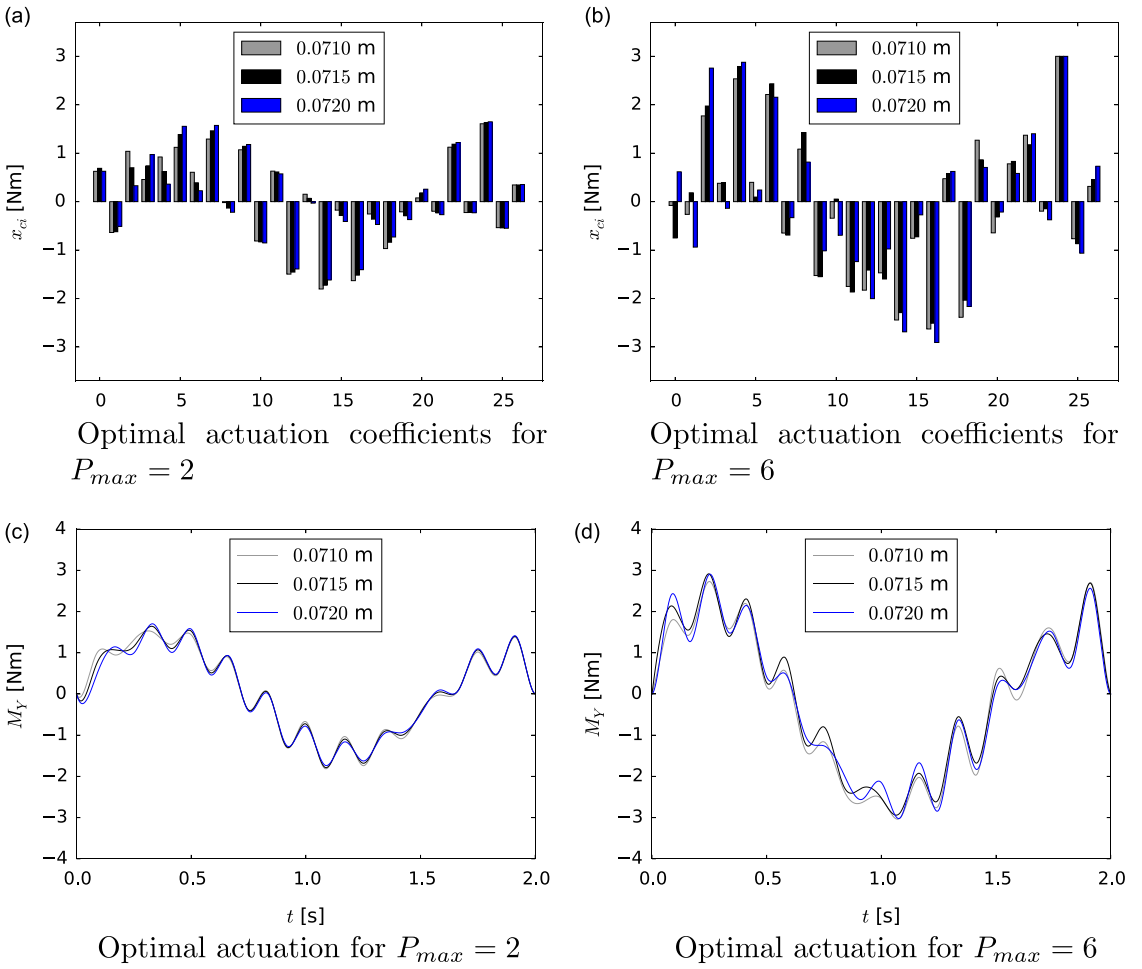

Fig. 17. Optimal control torque (parametrised with B-splines) for structural designs in the proximity of $l_{ref} = 0.0715$ m for small ($P_{\max} = 2$) and large ($P_{\max} = 6$) amplitude oscillations.

physical properties of the system. The performance gains with respect to the optimal control only case (DOE label in Tables 6 and 7) are as large as 45 percent, due to the switch from rigid to flexible-rigid body dynamics. This effect is clearly reflected by the development of a high frequency component in the optimal actuation signal (*zero* label in Fig. 14b). Also for the $f_{\max} = 6$ Hz case, where a mild level of resonance can already be induced on the initial design, the stiffness reduction achieved via co-design allows to better exploit it (compare the *DOE* and *zero* curves in Fig. 14a).

The dependency of the co-design derived optimal solution on the actuation bandwidth has important implications when a multi-resolution strategy (Section 3.4) is adopted to solve the co-design problem. When the combined optimisation is hierarchically solved using actuations of increasing bandwidth, in fact, the final structural design is driven by the bandwidth used to initialise the process. This is shown in more detail in Table 9, where the integrated multi-resolution design approach is demonstrated for a case in which the actuation is parametrised with a DSS. The optimisation is initiated using both a control bandwidth of 4 Hz and 6 Hz (stage 0): once the first combined optimisation is terminated, this is restarted after incrementing the maximum actuation frequency, $f_{\max}$, of 2 Hz. Note that at stage 0 structural design and actuation are as per the 4 Hz and 6 Hz bandwidth *zero* cases in Table 6.

When the multi-resolution process is started with a 6 Hz bandwidth actuation, *locking* between structural design and control force prevents any changes of the structural properties. Therefore, when a 12 Hz bandwidth is reached, the integrated design provided by the 12 Hz *zero* case in Table 6 is not retrieved. The final tip velocity value, $v_X(T)$, is, however, comparable as in both cases resonance is exploited. When the process is started from a 4 Hz bandwidth solution, on the other hand, structural design and actuation are not initially *locked* in a peak of resonance, being the bending natural frequency of the pendulum ($f_b = 4.27$) outside the actuation range. As a result, design and actuation are refined during the first stage and the final tip velocity of the pendulum, $v_X(T)$, increases by 7.1 percent. Once, however, structural design and actuation are *locked*, no further change is observed as the actuation bandwidth is increased.

The solutions in the multi-resolution process obtained from an initial 4 Hz bandwidth actuation in Table 9 can be compared against the corresponding co-design solutions in Table 6. In all cases, the final tip velocities and the level of

Table 9
Results of the combined optimisation using a multi-resolution strategy and a DSS parametrisation. Two different actuation bandwidth of 4 Hz and 6 Hz has been chosen to start the process.

Case	Stage	N_c	$f_{\max}$ (Hz)	l_3 (m)	f_b (Hz)	$v_X(T)$ (m s^{-1})
Initial bandwidth of 4 Hz	0	16	4	0.0550	4.27	10.61
	1	24	6	0.0584	4.53	13.44
	4	48	12	0.0584	4.53	13.44
Initial bandwidth of 6 Hz	0	24	6	0.0739	5.73	13.70
	3	48	12	0.0739	5.73	13.70

actuation are very similar. However, the structural design obtained via multi-resolution is consistently more flexible, showing that the initial actuation bandwidth has a clear impact on the final structural design.

Overall, the results obtained using a zero starting condition for the actuation prove the potential of adopting a gradient based co-design approach even for resonant, strongly nonlinear systems. On the one hand, and similar to what was observed with a sequential optimisation strategy (Section 4.1), the occurrence of structural-actuation *locking* around peaks of resonance can limit the progress of the optimisation, especially when a large bandwidth is used. This means that some initial sampling of the structural domain needs to be performed. On the other hand, however, co-design allows to explore much larger portions of the design space, even when this implies a drastic change in the system dynamics (such as those switching from a rigid to a flexible-rigid body dynamics). The rate of sampling of the structural design space, or conversely the overall number of co-design solutions to be found, can, thus, be conveniently reduced, facilitating the exploration of larger portions of the design space as compared to a zero order or traditional sequential optimisation approaches.

5. Conclusions

The control vector parametrisation technique has been used to solve a nonlinear optimal control problem, defined on a very flexible structure, and to explore the co-design process of open-loop control and structural properties of the system. The problem has been chosen to represent key features of the control of very flexible structures and a gradient method has been used to drive the optimisation. The control has been modelled using B-splines and DSS to test the effect of using local and global sets of basis functions. In both the optimal control and the co-design cases the time–frequency resolution of the parametrisations has been shown to be the most relevant factor driving the design.

In the optimal control problems, both the effect of an increasing rigid-flexible body dynamics coupling and the impact of the problem definition on the optimisation outcome have been investigated. The process has been demonstrated to capture and exploit the structural resonances, regardless of the level of nonlinearity shown by the system. The actuation cost has been measured by means of a quadratic force regulator term and included in the problem firstly via penalty augmentation and then via constraint enforcement. In the first case, a dependency of the optimal control on the path taken by the optimiser — which increases with the system nonlinearity — has been found. The constraint enforcement approach has allowed, instead, to produce more consistent results across parametrisations, as it drives the optimal control to reach the maximum admissible level of actuation.

An assessment of the impact of the parametrisation on the optimal control solution process has also been carried out. A transition region, in which the different reconstruction properties of splines and DSS leads to a gap in the final achievable performance, was identified. Elsewhere a good consistency across parametrisations has been found, particularly for low-medium levels of actuation and, thus, moderate nonlinear effects, while increasing the authority of the control leads to multiple local peaks of resonance. In this last case, the design space was found to be particularly non-smooth, causing the optimisation process to converge slowly, particularly when using global basis. A multi-resolution strategy has been proposed in these cases to make the process more efficient.

In the co-design problem, the system flexibility was allowed to vary while defining the actuation law itself. We have shown that co-design attempts starting from a previously computed optimal control solution (which are equivalent to a sequential design approach) do not result in relevant changes to structure size and control law. Once tuned on the same resonance/excitation frequency, structure and control *lock* in the initial design.

Designing the control law from zero has the great advantage of avoiding *locking* and, thus, allowing to move through larger portions of the design space. The high level of nonlinear effects nearby resonance regions has been shown to affect the convergence speed of the optimisation. The phenomenon, connected to the increased sensitivity of the control law with respect to changes in the structural design, requires a two-stage strategy — via solution of a pure optimal control problem — to fully complete the process.

The key element in the co-design process is the actuation time–frequency resolution. When the control bandwidth is larger than the structure bending mode natural frequency, the gradient based optimiser drives, as expected, the structural design towards the nearest peaks of resonance. However, when using a lower bandwidth control, performance is drastically improved with both parametrisations. Larger portions of the design space can be explored and the combined optimisation

has always managed to successfully drive the structural design in a region where the control could exploit the coupled rigid-flexible dynamics. While the portability of the approach when dealing with more complex structural systems — e.g. whose dynamics is driven by more modes of vibration — still requires a further assessment, these results prove the potential of gradient based co-design in vibrations control and structural dynamics, even for highly nonlinear problems.

Acknowledgements

The authors acknowledge the support of the UK Engineering and Physical Science Research Council (EPSRC), including an access grant to ARCHER, the UK National Supercomputing Service. All results in this paper are available as open data. Information on access can be found at http://www.imperial.ac.uk/aeroelastics/software.

References

[1] J. Allison, D.R. Herber, Multidisciplinary design optimization of dynamic engineering systems, *AIAA Journal* 52 (4) (2014) 691–710, http://dx.doi.org/10.2514/1.J052182.
[2] H. Fathy, J. Reyer, P. Papalambros, A. Ulsoy, On the coupling between the plant and controller optimization problems, *Proceedings of the American Control Conference*, Arlington, 2001, pp. 1864–1869.
[3] J.R.R.A. Martins, A.B. Lambe, Multidisciplinary design optimization: a survey of architectures, *AIAA Journal* 51 (9) (2013) 2049–2075, http://dx.doi.org/10.2514/1.J051895.
[4] J. Onoda, R. Haftka, An approach to structure/control simultaneous optimization for large flexible spacecraft, *AIAA Journal* 25 (8) (1987) 1133–1138.
[5] S.S. Rao, Combined structural and control optimization of flexible structures, *Engineering Optimization* 13 (1) (1988) 1–16, http://dx.doi.org/10.1080/03052158808940943.
[6] H. Asada, J. Park, S. Rai, A control-configured flexible arm: integrated structure control design,, *Proceedings of the 1991 IEEE International Conference on Robotics and Automation*, Sacramento, California, 1991, pp. 2356–2362, http://dx.doi.org/10.1109/ROBOT.1991.131755.
[7] Z. Xianmin, L. Jianwei, S. Yunwen, Simultaneous optimal structure and control design of flexible linkage mechanism for noise attenuation, *Journal of Sound and Vibration* 299 (4–5) (2007) 1124–1133, http://dx.doi.org/10.1016/j.jsv.2006.08.002.
[8] N. Alujević, G. Zhao, B. Depraetere, P. Sas, B. Pluymers, W. Desmet, H2 optimal vibration control using inertial actuators and a comparison with tuned mass dampers, *Journal of Sound and Vibration* 333 (18) (2014) 4073–4083, http://dx.doi.org/10.1016/j.jsv.2014.04.038.
[9] H. Nishigaki, K. Kawashima, Motion control and shape optimization of a suitlike flexible arm, *Structural Optimization* 15 (1998) 163–171.
[10] J.B. Cardoso, P.P. Moita, A.J. Valido, Design and control of nonlinear mechanical systems for minimum time, *Shock and Vibration* 15 (3–4) (2008) 315–323, http://dx.doi.org/10.1155/2008/741205.
[11] J.T. Allison, T. Guo, Z. Han, Co-design of an active suspension using simultaneous dynamic optimization, *Journal of Mechanical Design* 136 (8) (2014) 14, http://dx.doi.org/10.1115/1.4027335.
[12] S. Haghighat, J.R.R.A. Martins, H.H.T. Liu, Aeroservoelastic design optimization of a flexible wing, *Journal of Aircraft* 49 (2) (2012) 432–443, http://dx.doi.org/10.2514/1.C031344.
[13] T. Jackson, E. Livne, Integrated aeroservoelastic design optimization of actively controlled strain-actuated flight vehicles, *AIAA Journal* 52 (6) (2014) 1105–1123, http://dx.doi.org/10.2514/1.J050941.
[14] D. Trivedi, D. Dienno, C. Rahn, Optimal, model-based design of soft robotic manipulators, *Journal of Mechanical Design* 130 (9) (2008) 091402, http://dx.doi.org/10.1115/1.2943300.
[15] V. Etxebarria, A. Sanz, I. Lizarraga, Control of a lightweight flexible robotic arm using sliding modes, *International Journal of Advanced Robotic Systems* 2 (2) (2005) 103–110.
[16] S. Dwivedy, P. Eberhard, Dynamic analysis of flexible manipulators, a literature review, *Mechanism and Machine Theory* 41 (7) (2006) 749–777, http://dx.doi.org/10.1016/j.mechmachtheory.2006.01.014.
[17] C.E. Cesnik, R. Palacios, E.Y. Reichenbach, Reexamined structural design procedures for very flexible aircraft, *Journal of Aircraft* 51 (5) (2014) 1580–1591, http://dx.doi.org/10.2514/1.C032464.
[18] T. Önsay, A. Akay, Vibration reduction of a flexible arm by time-optimal open-loop control, *Journal of Sound and Vibration* 147 (2) (1991) 283–300, http://dx.doi.org/10.1016/0022-460X(91)90716-W.
[19] L.T. Biegler, *Nonlinear Programming, Concept, Algorithms, and Applications to Chemical Processes*, SIAM, Philadelphia, 2010.
[20] M. Schlegel, K. Stockmann, T. Binder, W. Marquardt, Dynamic optimization using adaptive control vector parameterization, *Computers & Chemical Engineering* 29 (8) (2005) 1731–1751, http://dx.doi.org/10.1016/j.compchemeng.2005.02.036.
[21] B.C. Fabien, Piecewise polynomial control parameterization in the direct solution of optimal control problems, *Journal of Dynamic Systems, Measurement, and Control* 135 (3) (2013). http://dx.doi.org/10.1115/1.4023401.
[22] Q. Lin, R. Loxton, K.L. Teo, The control parameterization method for nonlinear optimal control: *a survey*, *Journal of Industrial and Management Optimization* 10 (1) (2013) 275–309, http://dx.doi.org/10.3934/jimo.2014.10.275.
[23] D.H. Hodges, A. Mixed, Variational formulation based on exact intrinsic equations for dynamics of moving beams, *International Journal of Solids and Structures* 26 (11) (1990) 1253–1273, http://dx.doi.org/10.1016/0020-7683(90)90060-9.
[24] M. Geradin, A. Cardona, *Flexible Multibody Dynamics: A Finite Element Approach*, John Wiley & Sons Ltd, Chichester, UK, 2001.
[25] H. Hesse, R. Palacios, Reduced-order aeroelastic models for dynamics of maneuvering flexible aircraft, *AIAA Journal* 52 (2014) 1–16, http://dx.doi.org/10.2514/1.J052684.
[26] R. Palacios, Nonlinear normal modes in an intrinsic theory of anisotropic beams, *Journal of Sound and Vibration* 330 (8) (2011) 1772–1792, http://dx.doi.org/10.1016/j.jsv.2010.10.023.
[27] C. de Silva, *Vibration and Shock Handbook*, CRC Press, Boca Raton, Florida, USA, 2005.
[28] D. Kraft, A Software Package for Sequential Quadratic Programming, Technical Report, DLR German Aerospace Center Institute for Flight Mechanics, Köln, Germany, 1988.
[29] J. Murua, R. Palacios, J.M.R. Graham, Applications of the unsteady vortex-lattice method in aircraft aeroelasticity and flight dynamics, *Progress in Aerospace Sciences* 55 (2012) 46–72, http://dx.doi.org/10.1016/j.paerosci.2012.06.001.
[30] J.S. Gray, K.T. Moore, T.A. Hearn, B. Naylor, Standard platform for benchmarking multidisciplinary design analysis and optimization architectures, *AIAA Journal* 51 (10) (2013) 2380–2394, http://dx.doi.org/10.2514/1.J052160.
[31] Q. Wang, W. Yu, Sensitivity analysis of geometrically exact beam theory (GEBT) using the adjoint method with hydra, *The 52nd AIAA/ASME/ASCE/AHS/ASC Structures, Structural Dynamics and Materials Conference*, Denver, Colorado, 2011, pp. 1–15.
[32] M. Sabatini, P. Gasbarri, G.B. Palmerini, R. Monti, Operational modal analysis via image based technique of very flexible space structures, *Acta Astronautica* 89 (2013) 139–148, http://dx.doi.org/10.1016/j.actaastro.2013.04.005.